JOC The Journal of Organic Chemistry

Article

pubs.acs.org/joc

Preparation and pH-Switching of Fluorescent Borylated Arylisoquinolines for Multilevel Molecular Logic

Vânia F. Pais,[†] Mauricio Lineros,[†] Rocío López-Rodríguez,[‡,∥] Hamdy S. El-Sheshtawy,[§] Rosario Fernández,[∥] José M. Lassaletta,[‡] Abel Ros,*[,‡] and Uwe Pischel*[,†]

[†]CIQSO—Center for Research in Sustainable Chemistry and Department of Chemical Engineering, Physical Chemistry, and Organic Chemistry, University of Huelva, Campus de El Carmen s/n, 21071 Huelva, Spain

[‡]Institute for Chemical Research (CSIC-US), C/Américo Vespucio 49, 41092 Seville, Spain

[§]Chemistry Department, Faculty of Science, South Valley University, 83523 Qena, Egypt

[∥]Department of Organic Chemistry, University of Seville, C/Prof. García González 1, 41012 Seville, Spain

Supporting Information

ABSTRACT: The preparation of pH-switchable fluorescent borylated arylisoquinoline dyes via a flexible iridium-catalyzed route is reported. The obtained dyes feature aromatic amino substitution and lateral aliphatic amino groups as electron donors. The photophysical properties of the internal charge transfer dyes were studied, which was complemented by density functional theory calculations. Appreciable fluorescence quantum yields (Φ_f up to ca. 0.4) and characteristic spectral fingerprints in the green to red emission range were observed. The fluorescence modulation upon multiple and orthogonal protonation with triflic acid was studied and led to the interpretation of multilevel switching including *off*–*on*–*off*, ternary, and quaternary responses.

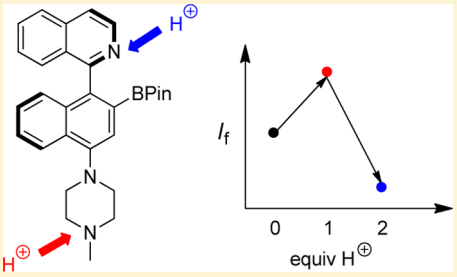

INTRODUCTION

The design of molecular and supramolecular switches that change their fluorescence properties upon interaction with chemical inputs is not only an academically rewarding exercise but has also contributed decisively to the enormous success of chemosensing in analytical chemistry applications in environmental sciences, life sciences, and clinical diagnostics.[1−5] The measurement of pH by means of fluorescent probes is a simple but instructive example for the conceptual approach to fluorescence switching. In the majority of cases, the electronic properties of electron donors and acceptors that are integrated with the fluorophore architecture are modulated by protonation. This may give rise to fluorescence enhancement or quenching as well as to ratiometric responses. The change of the optical reporter signal can be straightforwardly translated into switching between *off* and *on* states, which are verbal descriptions of binary 0 or 1, respectively. This conceptual analogy has paved the way to interpret the functions of such switches in terms of molecular information processing and logic.[6−12] While simple *off*–*on* (signal enhancement) or *on*–*off* (quenching) fluorescence switching by pH modulation is described abundantly in the literature, the design of more complex signal responses in the form of *off*–*on*–*off* or *on*–*off*–*on* patterns and interpretations beyond the binary 0 and 1 notation in the form of multivalued logic and memory remains a challenging task.[12,13] The combination of two antagonistic proton receptors with a fluorophore and photoinduced electron transfer (PET) as communication mechanism has given rise to a general strategy for *off*–*on*–*off* and also *on*–*off*–*on* switches.[14−20] The integration of *off*–*on*–*off* PET switches with polymeric materials[21−23] or in higher-order supramolecular structures such as micelles was demonstrated as well.[24−26] Some other designs included fluorescent or luminescent assemblies based on transition metal ion complexes with pH-switchable ligands where the modulation of the emission output signal was achieved by controlling PET and energy transfer (EnT).[27−32] All-photonic *off*–*on*–*off* switching, that is, switches that work exclusively with optical inputs and outputs, has been observed for other photophysical designs.[33,34] The variation of π-conjugation in purely organic systems was described as another viable mechanism to achieve *off*–*on*–*off* or *on*–*off*–*on* fluorescence switching.[35,36] Finally, acidochromic switching inspired by classical pH azobenzene-based indicators has been used for the implementation of an *off*–*on*–*off* chromogenic response.[37] While the previously described switches use multilevel input signals, for example, low, medium, and high proton concentrations, their output is read through a binary low–high (0–1) convention. On the other hand, fluorescent systems that allow for the reading of three or even four stable output states leading to ternary or quaternary switching are rather rare. Some of the few reported strategies toward this ambitious and nontrivial objective harnessed the switching of fluorophores by sequential modulation of excited state processes such as internal charge transfer (ICT), PET, and EnT. In this way *low*–*medium*–*high*[18]

Received: May 24, 2013
Published: July 30, 2013

   dx.doi.org/10.1021/jo401147t | J. Org. Chem. 2013, 78, 7949−7961

Scheme 1. Structures of BAI Dyes 1−4 and Their Nonborylated Analogues M1−M4

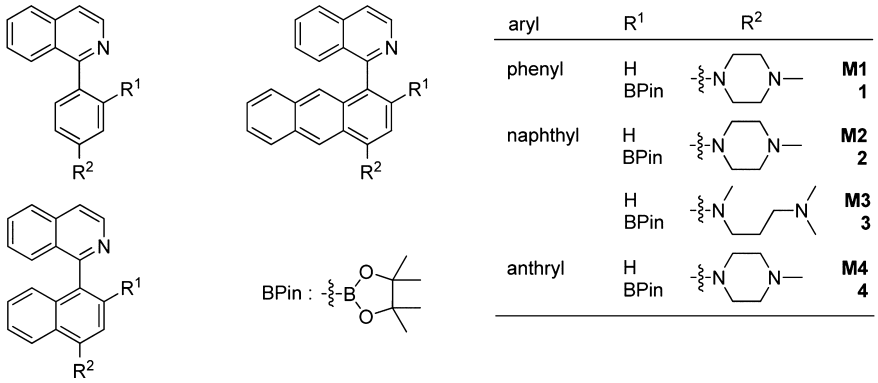

as well as the inverse sequence[38] were demonstrated. Other approaches include the protonation and deprotonation of fluorescent ligands that are integrated in metal ion coordination complexes,[39,40] the pH-control of polyamine−fluorophore conjugates,[41] and the exploitation of excited-state proton transfer.[41] An example for a Zn(II) input-driven ternary switch showing a *medium−off−on* fluorescence output sequence based on a squaraine dye was reported as well.[42]

In the present study the aim of our research was the modular design of multilevel switches based on the class of fluorescent borylated arylisoquinoline (BAI) dyes (see general structure in Scheme 1), recently introduced by us. In a previous work[43] we have shown that the presence of the boronic ester substituent modulates the electronic properties and consequently the observation of ICT fluorescence in a rather advantageous manner (good quantum yields and fine-tuned emission covering a large part of the visible spectrum). The multiresponsive features of BAI dyes were exploited through the protonation of the isoquinoline moiety and the formation of an *ate* complex between the trivalent boron center and fluoride ions.[44,45] Interestingly, in the context of switching, triarylboron compounds were shown to yield three spectrally differentiated fluorescent states through the application of protons and fluoride ions inputs.[46] However, as an important difference and as explored in the examples discussed previously, we concentrate herein on switches that generate bi- and multistable fluorescence output responses as a function of a *single* input signal (protons) that is applied at different concentration levels.

To this end we prepared a series of amino-substituted BAI dyes (see Scheme 1) that behave as organic fluorescent polybases. We were able to show that the control of the electronic structure of the dyes can effectively lead to new molecular entities behaving as *off−on−off* and *on−off−on'* switches as well as ternary and quaternary switches with potential for information processing.[12]

RESULTS AND DISCUSSION

Synthesis of the Borylated Arylisoquinolines 1−4 and Their Nonborylated Model Chromophores. The nonborylated compounds **M1**−**M4**, which served also as photophysical models (see following sections), were used as precursors of the borylated title compounds. The synthesis of the nonborylated arylisoquinolines as well as their borylated derivatives is summarized in Scheme 2. Starting from the previously reported compound **A1**, the nucleophilic substitution of the methoxy group with lithium 4-methylpiperazin-1-ide[47] afforded compound **M1** in 76% yield. The same methodology was applied analogously in the synthesis of the nonborylated arylisoquinolines **M2** and **M3**. The nucleophilic substitution of 1-(8-methoxynaphthalen-1-yl)isoquinoline[43] with the corresponding lithium amides afforded the products **M2** and **M3** with a yield of 68% and 73%, respectively. This methodology (method B, Scheme 2b) provides a useful alternative to Buchwald's methodology[48] that is based on a palladium-catalyzed one-pot borylation/Suzuki coupling starting from the corresponding haloarenes (method A, Scheme 2b). In the concrete case of compound **M2**, the latter method gave the product with only 17% yield.[43] Compound **M4** was synthesized in a synthetic sequence (Scheme 2d) that started with the preparation of **A4** (86% yield) from 1-chloroanthracene and *N*-methylpiperazine using a palladium-catalyzed Buchwald−Hartwig coupling. The subsequent regioselective bromination at the 4-position of **A4**, followed by a palladium-catalyzed one-pot borylation/Suzuki coupling[48] of **B4** with 1-chloroisoquinoline, gave compound **M4** in 31% yield.

The introduction of the boronic ester substituent was carried out following a methodology recently reported by some of us that is based on the iridium(III)-catalyzed nitrogen-directed ortho-borylation of arylisoquinolines.[49,50] The herein-exploited compounds **1**−**4** were obtained with this method in very good to excellent yields. The reaction worked well at 55 °C, affording the desired ortho-borylation products **2** and **4** in 61% and 80% yield, respectively (Scheme 2e). The borylation of the substrates **M1** and **M3** required elevated reaction temperatures (80 °C) to afford the desired borylated products **1** and **3** in 89% and 58% yield, respectively. The need for higher temperatures can be attributed to the low C−H bond acidity of **1** and to the ability of the NMe_2 group of **3** to compete with the N(sp^2) atom of the isoquinoline for the vacant coordination site of the catalyst.[51] The ^{1}H NMR and ^{11}B NMR analyses revealed unambiguously that internal B−N interactions are clearly dependent on the steric hindrance around the central bond between the isoquinoline and the aryl moiety. On the one hand, the hindered products **2**−**4** showed no B−N interaction which can be identified by the ^{1}H NMR signals of the diastereotopic pinacol methyl groups, having two singlet resonances at 0.74−0.94 ppm. On the other hand, for the unhindered product **1**, an internal B−N interaction was inferred because the pinacol methyl groups were equivalent and appeared as a single resonance at 1.41 ppm. These assignments were further confirmed by the ^{11}B NMR spectra of the products: the hindered products **2**−**4** showed a signal in the 31−32 ppm range, while for compound **1** the B−N interaction resulted in a strong shielding, and the signal appeared upfield

dx.doi.org/10.1021/jo401147t | J. Org. Chem. 2013, 78, 7949−7961

Scheme 2. Synthesis of BAI Dyes 1−4 and Their Nonborylated Analogues M1−M4

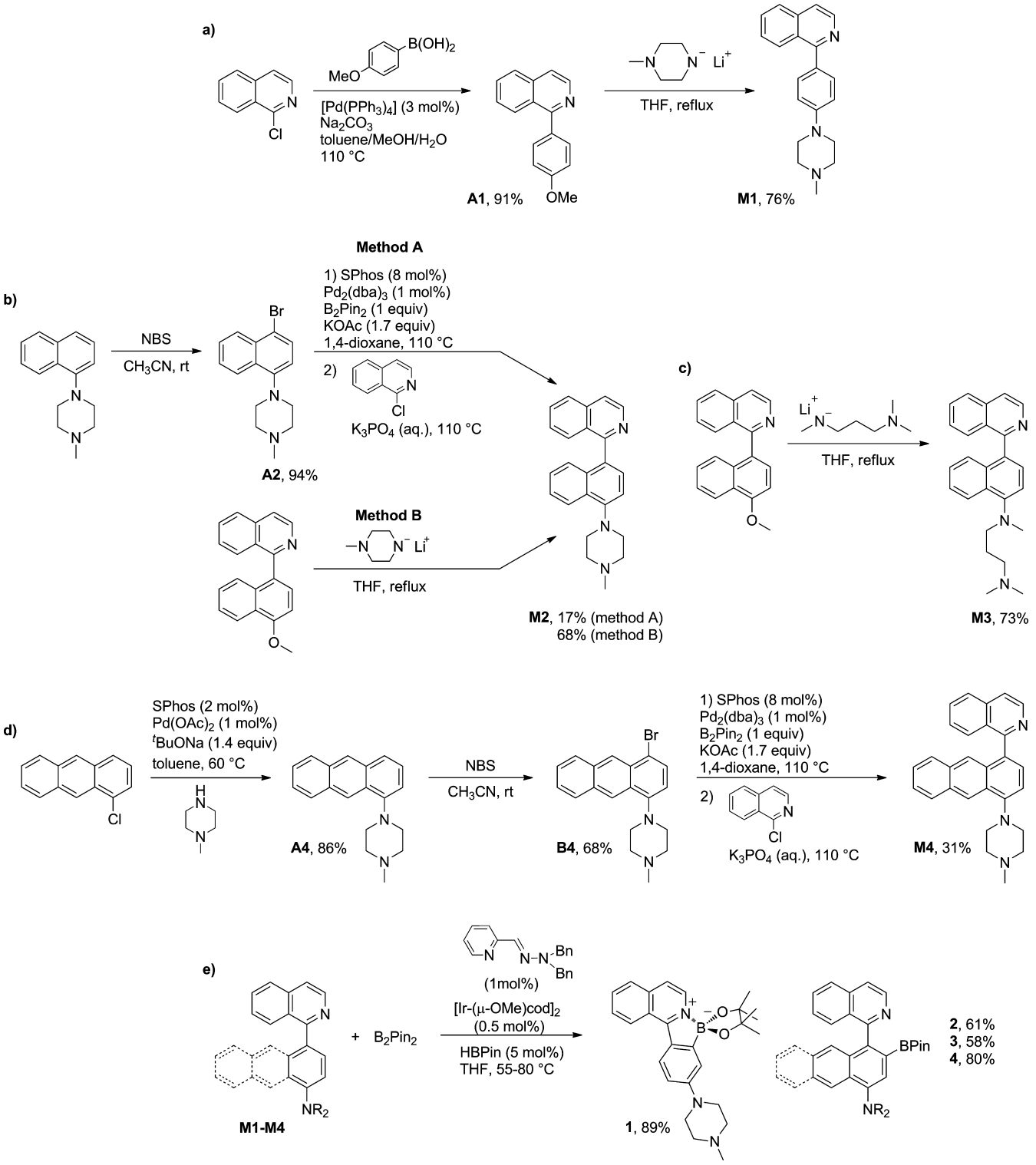

shifted at 13 ppm. These observations are in agreement with reported data for both types of boron atoms, that is, tricoordinated B (dyes **2**−**4**) and tetra-coordinated B (dye **1**).[52]

Molecular Design Principle for Multiple Fluorescence Switching. BAI dyes show fluorescence emission which originates from an ICT state. This has been recently demonstrated by us for an extended series of BAI dyes by time-dependent density functional theory (TD-DFT) calculations, the observation of characteristic solvatochromic effects, and the conclusive correlation between redox and emission properties.[43] TD-DFT calculations revealed the same ICT phenomena also for the herein-investigated dyes: in general (with the exception of dye **4**) the highest occupied molecular orbital (HOMO) is mainly located on the borylated aminoaryl electron donor moiety, while the lowest unoccupied molecular orbital (LUMO) involves mainly the isoquinoline part (electron acceptor) (see following sections).

dx.doi.org/10.1021/jo401147t | J. Org. Chem. 2013, 78, 7949−7961

BAI dyes **1**–**4** contain various orthogonal protonation sites: (a) a lateral tertiary amine is the most basic moiety (typical pK_a ca. 8–10 in water, for example, pK_a ca. 8.4 for 1,4-dimethylpiperazine)[53] and (b) the less basic isoquinoline moiety (pK_a ca. 4.8 for parent isoquinoline in 1/1 methanol/water).[54] The nitrogen at the aryl ring could also be protonated (in fact only observed for dye **3**; see following), giving rise to a third protonation site. However, the latter nitrogen is evidently the least basic site because of the involvement of its lone pair in the ICT process and the electrostatic repulsion caused by the neighboring protonated lateral amino function.

The orthogonal protonation behavior of the investigated BAI dyes is illustrated by the representative example of dye **2**. The ^{1}H NMR spectra were observed as a function of the added equivalents of triflic acid (TfOH; CF_3SO_3H) (see Figure 1).

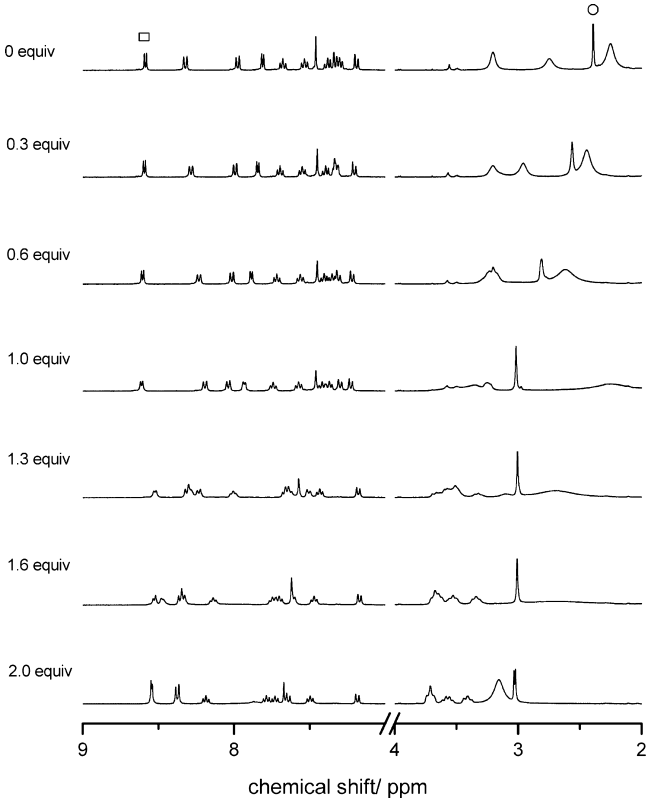

Figure 1. ^{1}H NMR spectra of dye **2** in acetonitrile-d_3 upon successive addition of TfOH (0–2 equiv). The square marks the proton in the ortho position relative to the isoquinoline N; the circle marks the N–CH_3 protons of the piperazinyl unit; see discussion in text.

Upon addition of 1 equiv of TfOH, it was clearly seen that the N–CH_3 methyl protons were downfield shifted ($\Delta\delta$ = +0.62 ppm), while the aromatic protons were much less or not at all affected. This is indicative of the exclusive protonation of the lateral aliphatic amino group in the first step. As expected, the protons of the piperazinyl methylene neighboring the N–CH_3 group (α-CH_2) were also downfield shifted by ca. 0.6 ppm (merging with the signal of the methylene protons closer to the N at the aryl residue; β-CH_2) on addition of the first equivalent of TfOH. With increasing amounts of acid (>1.0 equiv) the β-CH_2 protons suffered downfield shifts as well, and signal splitting for both the α- and β-CH_2 groups was seen. The addition of a second equivalent of TfOH led to pronounced and rather complex changes in the aromatic region of the ^{1}H NMR spectrum. However, by selecting the signal of the proton ortho to the isoquinoline N as indicator, a very clear trend was notable: until 1 equiv was added, this signal did not change, while in the course of the addition of a second equivalent of TfOH, a clear upfield shift and a merge with other aromatic proton signals resulted. In conclusion, in agreement with the pK_a values of the basic sites in dye **2**, the first equivalent of acid led to the protonation at the lateral aliphatic amino N, while the second acid equivalent protonated the isoquinoline N.

The polybasic behavior enabled the sequential pH control of the electronic properties that guide ICT processes as well as PET involving the lateral aliphatic amino group. This resulted consequently in a modulation of the fluorescence response. This photophysical scenario is schematically summarized in Scheme 3 and will be discussed case-by-case for the investigated dyes **1**–**4** (see following sections).

Scheme 3. Mechanistic Proposal for Excited-State Interactions in the BAI Dyes 1–4

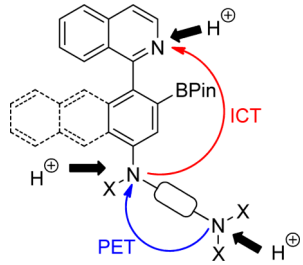

DFT Calculations. To establish the ICT character of the investigated dyes **1**–**4**, DFT calculations were performed. The ground state geometries (see Supporting Information) were optimized by the application of the Kohn–Sham DFT with the Becke 3 Lee–Yang–Parr (B3LYP) hybrid functional method and the 6-31+G(d,p) basis set. The energy-minimized structures of the BAI dyes **2**–**4** revealed a nearly perpendicular positioning of the isoquinoline ring with respect to the aryl residue (tilt angles: 86.7° for **2**, 84.6° for **3**, and 86.5° for **4**). The distance between the isoquinolyl N and the B atom was measured as being between 3.52 and 3.55 Å for these three dyes. This distance is slightly larger than the sum of the van der Waals radii of B (1.92 Å) and N (1.55 Å),[55] indicating the absence of interaction between the Lewis acid and base centers. This notion agrees with the observations made by ^{11}B NMR spectroscopy (see previous sections), which clearly supported the absence of B–N coordinative bonding for the dyes **2**–**4**. However, in the case of dye **1**, for which ^{11}B NMR predicted a tetra-coordinated B (see previous sections), the optimized geometry showed a tilt angle of 59.0°, smaller than the ones obtained for the compounds **2**–**4**. This resulted in a significantly reduced B–N distance of 3.21 Å, which is shorter than the sum of the van der Waals radii and thereby supports the notion of the formation of an intramolecular Lewis pair.

The frontier molecular orbitals were calculated by application of the TD-DFT at the B3LYP/6-31+G(d,p) level of theory. The corresponding contour plots of the HOMO and the LUMO for each dye and the molecular orbital energies are shown in Figure 2. For the BAI dyes **1**–**3** the HOMO was located on the amino-substituted aryl electron donor moiety, while the LUMO had its largest contribution from the isoquinoline residue, functioning as electron acceptor in the ICT process. The anthracene-substituted dye **4** was an

dx.doi.org/10.1021/jo401147t | J. Org. Chem. 2013, 78, 7949–7961

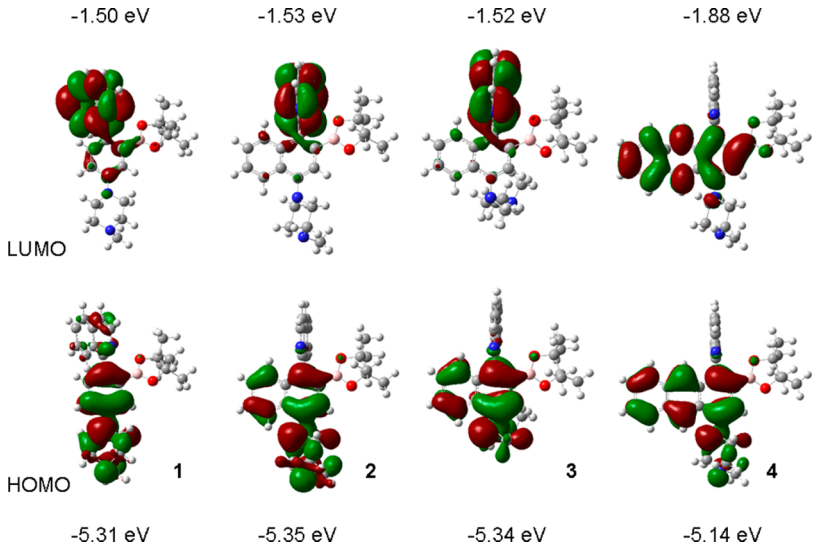

Figure 2. HOMO−LUMO contour plots and orbital energies of dyes **1**−**4**.

exception. Here the HOMO was located on the piperazinyl−anthryl donor moiety, and the LUMO was on the borylated anthryl electron acceptor residue, pointing to a more locally excited state. However, the LUMO+1 (which lies close to the LUMO) orbital (−1.54 eV) of dye **4** had its major contribution from the isoquinoline moiety (see Supporting Information), akin to the observations made for the LUMOs of the dyes **1**−**3**. For these reasons, the ICT character of dye **4** was similar to that of the other dyes. This has been confirmed independently by the observation of a solvatochromic effect.[S6]

On the one hand, the absolute HOMO and LUMO gas-phase energies for compounds **1**−**3** were situated at ca. −5.3 eV and ca. −1.5 eV, respectively, leading to an energy gap of ca. 3.8 eV (see Figure 2). On the other hand, dye **4** showed a reduced energy gap of ca. 3.3 eV (see Figure 2), which coincides with the fact that this dye also showed the most red-shifted fluorescence emission (see following sections).

Photophysical Properties. The UV−vis absorption and fluorescence properties of the BAI dyes **1**−**4** in acetonitrile solution are summarized in Table 1, and the corresponding spectra are shown in Figure 3. Dyes **2** and **3** showed UV−vis absorption bands at a maximum around 323 nm, typical for substituted naphthalenes and isoquinolines. The anthracene-derived dye **4** showed an absorption peak at 321 nm (isoquinoline) and a red-shifted band with two maxima at 388 and 401 nm. The UV−vis absorption spectrum of dye **1** had, at first glance, a surprisingly broad absorption band at 420 nm. This can be ascribed to neither the phenyl moiety nor the isoquinoline. However, one must bear in mind that the intramolecular formation of a Lewis pair through the unequivocally evidenced B−N interaction further increases the electron density at the piperazinyl−phenyl moiety and also turns the isoquinoline into a stronger electron acceptor. This provides an explanation for the observation of this spectral feature which we ascribe to a ground-state charge-transfer band. The ICT character of the fluorescent state of the herein-investigated dyes is well supported by the general observation of broad and rather red-shifted emission bands ($\lambda_{f,max}$ between 560 and 638 nm). For ICT a trend relationship between the emission energy (as rated by the maximum of the fluorescence band) and the electron donating character of the piperazinyl-substituted aryl moieties is expected.[43] It was gratifying to

Table 1. Photophysical Properties of the BAI Dyes 1−4 and Their Protonated Forms in Acetonitrile

	$\lambda_{abs,\,max}$, nm	ε, $M^{-1}cm^{-1}$[a]	$\lambda_{f,\,max}$, nm	Φ_f	τ_f, ns[b]
1	420	12300	559	0.07	0.65 (82%), 6.64 (18%)
1H$^+$	400	10200	530	0.45	5.60
1H$_2^{2+}$	370	5300	537	0.01	1.15 (18%), 5.67 (82%)
2	323	9600	599	0.37	5.44
2H$^+$	311, 322	9800	576	0.50	7.09
2H$_2^{2+}$	327, 340	9800	*c*	*c*	*c*
3	323	7500	607	0.35	6.01
3H$^+$	323	8000	600	0.39	6.88
3H$_2^{2+}$	340	9100	*c*	*c*	*c*
3H$_3^{3+}$	333, 340	6400	447	0.03	1.24
4	388, 401	5400	526, 638	0.23	4.87
4H$^+$	380, 399	5400	502, 622	0.20	4.05
4H$_2^{2+}$	342, 388, 406	5900	502	0.01	11.00

[a]The molar absorption coefficient refers to the longest-wavelength absorption maximum. [b]The lifetime of the major component (≥95%) is shown except for the cases where two exponentials contributed significantly. [c]Nonfluorescent species.

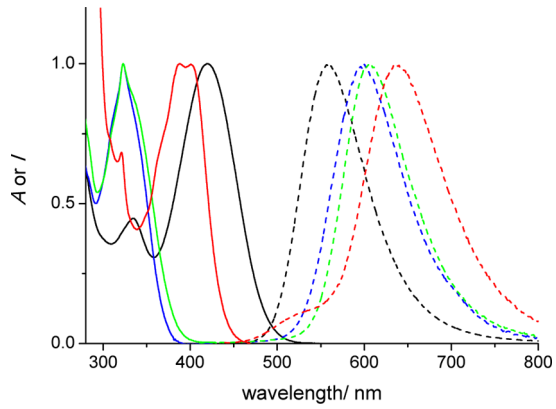

Figure 3. UV−vis absorption (solid lines) and fluorescence spectra (dashed lines) of the investigated BAI dyes in acetonitrile: black, **1**; blue, **2**; green, **3**; red, **4**.

dx.doi.org/10.1021/jo401147t | J. Org. Chem. 2013, 78, 7949−7961

observe that dye **4** showed the most red-shifted emission in the investigated series because the piperazinyl−anthryl unit is assumed to be the easiest one to oxidize. The somewhat blue-shifted emission maxima of the naphthalene-containing dyes **2** and **3** followed this rationalization. Dye **1**, containing the most difficult to oxidize aryl residue, showed expectedly the lowest emission wavelength maximum. However, in comparison to dyes **2**−**4**, it was still higher than may be expected. This is clearly related to the ground state B−N interaction in **1** (see previous sections), which turns the aryl residue into a better electron donor and the isoquinoline into a better electron acceptor. Hence, the resulting excited ICT state is expected at relatively low energy, corresponding to the red-shifted emission.

The relatively low quantum yield of Φ_f = 0.07 of dye **1** is a consequence of a relatively efficient PET from the lateral N of the piperazinyl substituent (see discussion following). On the other hand, dyes **2**−**4** showed yellow to orange emission colors (see Figure 4) with quite significant quantum yields (Φ_f = 0.23−0.37), pointing to less strong PET effects. In the case of dye **4**, which has a quite low-lying ICT state, the enhanced nonradiative deactivation as consequence of the energy gap law contributes to the somewhat lower quantum yield as compared to dyes **2** and **3** (see Table 1). The fluorescence lifetimes for dyes **2**−**4** varied between 4.87 and 6.01 ns. Compound **1** showed a much shorter lifetime of 0.65 ns (along with a minor component of 6.64 ns). This confirms the trend of a lower emission quantum yield of **1** as compared to the other dyes.

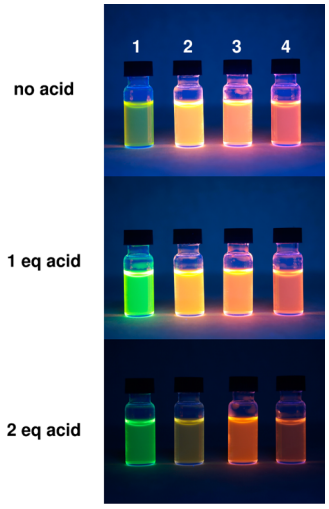

Figure 4. Color perception and brightness of the BAI dyes **1**−**4** in the absence of acid and in the presence of one or two equivalents TfOH in acetonitrile solutions.

The nonborylated arylisoquinolines **M1**−**M4** were included as model compounds in this study. In comparison to their borylated analogues the emission spectra of **M1**−**M4** were blue-shifted, and lower fluorescence quantum yields were obtained (see Table S1 in Supporting Information). These observations underline the crucial role of the boron-substitution in the excited-state behavior of dyes **1**−**4**. This is in agreement with the general observations made for other BAI dyes.[43] Interestingly, for dye **M1** also the UV−vis absorption spectrum changed dramatically. The missing possibility of intra-Lewis pair formation led to a blue shift of more than 80 nm for the longest-wavelength absorption band.

Effects of Protonation. As outlined previously, the BAI dyes **1**−**4** were designed to serve as proton-sensitive polybasic fluorescent switches. Noteworthy, the UV−vis absorption spectra corresponding to the acid titrations of the investigated dyes showed clear isosbestic points for the orthogonal protonation steps (see Figure 5a and 5b for the example of dye **1** and the Supporting Information for the other dyes). This hints of well-defined equilibria in the different phases of the titration, thereby supporting the previously discussed sequential protonation of the basic receptor sites. Interestingly, the long-wavelength absorption band of dye **1** showed a slight blue shift by ca. 20 nm upon the first protonation (see following discussion) and then vanished in the second protonation step of the isoquinoline in favor of a new band at ca. 370 nm. The disappearance of the B−N interaction in the second protonation, but not in the first one, was independently confirmed by ^{11}B NMR spectroscopy (see Supporting Information). These results are once more in agreement with the orthogonal protonation behavior for the herein-investigated dyes.

It was anticipated that the lateral aliphatic amino function would be able to engage in electronic interactions with the excited ICT state of the dye, possibly via PET (see Scheme 3). This would lead to ICT fluorescence quenching that can be inverted upon protonation as the result of the deactivation of the electron-donating amine. This assumption is based on the observations made for other ICT fluorophores with attached amino functions at their "donor sites".[4,57] Despite this potentially common mechanistic PET feature of the investigated dyes, quite variable photophysical effects were observed for the first protonation step (see Table 1 and the emission color changes depicted in Figure 4 for the different monoprotonated forms). In general, the efficiency of PET depends sensibly on the redox potentials of the involved electron donor (the amine) and acceptor (the BAI dye) as well as on the energy of the ICT state.[58] Given the variation of some of these parameters (especially the electron acceptor properties and ICT energies) in the investigated series of compounds, the differentiated response to protonation of the lateral electron-donating amine can be reasonably rationalized. In detail, for dye **1** a significant increase of the fluorescence quantum yield by a factor of ca. 6 was seen. This trend was also accompanied by the observation of a longer lifetime (see Table 1) and a much brighter emission perception (see Figure 4) as compared to the nonprotonated dye. Obviously, the protonation leads to the suppression of a quite efficient PET. The B−N interaction (see previous discussion) increases the ground-state electron acceptor character of the isoquinoline. Furthermore, the in comparison to the other dyes somewhat higher ICT state energy favors PET as well. As a side observation, the fluorescence maximum of $\mathbf{1H}^+$ was blue-shifted by ca. 30 nm, which is in line with a slight destabilization of the ICT state (see previous sections for a related effect in the UV−vis absorption spectrum of dye **1**). This may occur because of the sharing of the proton between the both piperazinyl N atoms and the consequent lowering of the electron donor strength of the N that is connected to the aryl moiety.[20] With respect to this "blue shift effect" for the monoprotonated form, similar observations were made for dyes **2** and **4** ($\Delta\lambda$ = 16−24 nm). The smallest blue shift ($\Delta\lambda$ = 9 nm) was seen for dye **3**, where the two N atoms are not as preorganized as in the conformationally more restricted piperazinyl. Returning to the discussion of the emission intensity changes upon monoproto-

dx.doi.org/10.1021/jo401147t | J. Org. Chem. 2013, 78, 7949−7961

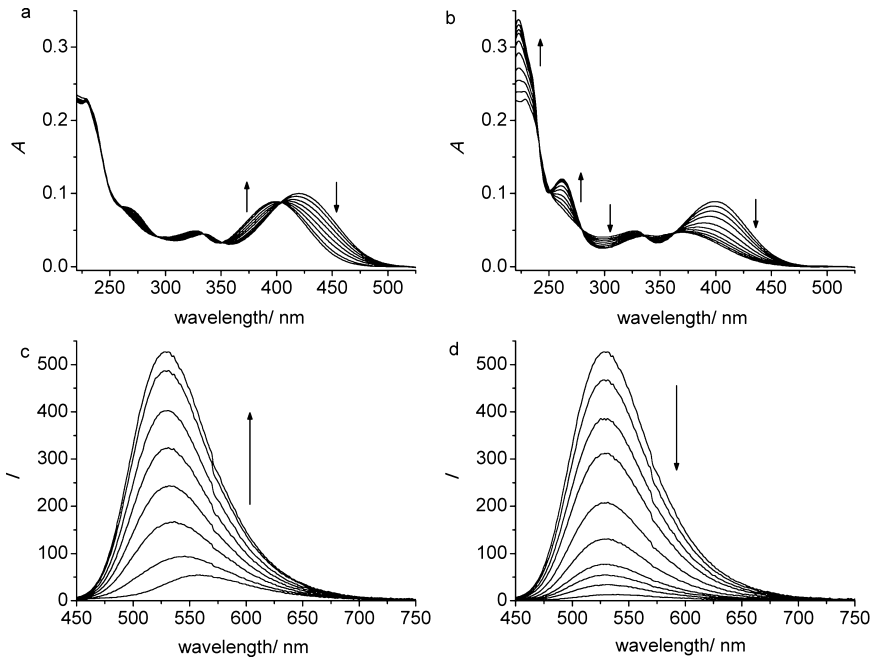

Figure 5. UV−vis absorption and fluorescence titration of dye **1** (8.2 μM) with TfOH in acetonitrile; (a) UV−vis spectra (0−1.0 equiv of TfOH), (b) UV−vis spectra (1.0−2.1 equiv of TfOH), (c) fluorescence spectra (0−1.0 equiv of TfOH); (d) fluorescence spectra (1.0−2.1 equiv of TfOH). The sample was excited at 336 nm (isosbestic point maintained throughout the complete titration).

nation, the fluorescence switching effects of dyes **2**−**4** were significantly different in comparison to compound **1**. Dye **2** yielded a smaller quantum yield enhancement factor [$\Phi_f(\mathbf{2H^+})/\Phi_f(\mathbf{2})$, ca. 1.4], but given the already significant fluorescence quantum yield in the absence of protons, the emission efficiency of $\mathbf{2H^+}$ is quite appreciable (Φ_f = 0.50). Dye **3** increased its fluorescence quantum yield by an even smaller factor [$\Phi_f(\mathbf{3H^+})/\Phi_f(\mathbf{3})$, ca. 1.1] and dye **4** did practically not change its emission quantum yield; see Table 1. For dyes **2**−**4** the PET effects are obviously weaker than they are for dye **1**. This may be because of the missing B−N interaction and the comparatively less strong electron-acceptor character of the isoquinoline part. However, some modest PET from the lateral amino N was observed for dyes **2** and **3**. In the case of dye **4**, the ICT state is too low-lying to favor any PET. The less dramatic changes of the quantum yields upon monoprotonation of dyes **2**−**4** are easily detected with the naked eye (see Figure 4).

The second protonation (addition of 2 equiv of TfOH), which happens at the isoquinolyl moiety, consistently yielded a practically quantitative quenching of the ICT fluorescence (see Table 1 and Figure 4). This has been observed and discussed recently by us for related BAI dyes.[43] The main reason for this effect is the increased acceptor strength of the protonated isoquinoline that leads to a rather low-lying ICT state. Presumably, this state, following the energy gap law, deactivates preferentially via nonradiative pathways. Dye **3** is different from the other dyes insofar as the third protonation step, this time at the N that is connected to the naphthyl residue, was observed. Such behavior is very unlikely for the monoprotonated piperazinyl unit in dyes **1**, **2**, and **4**, which would have to accommodate two positive charges in very close proximity. However, also for dye **3** a larger excess (20 equiv) was necessary to see the formation of $\mathbf{3H_3^{3+}}$. This species showed a strongly blue-shifted emission at a maximum of 450 nm (see Figure 6), indicative of an ICT that has been energetically destabilized by the excessive weakening of the electron donor strength of the protonated nitrogen.

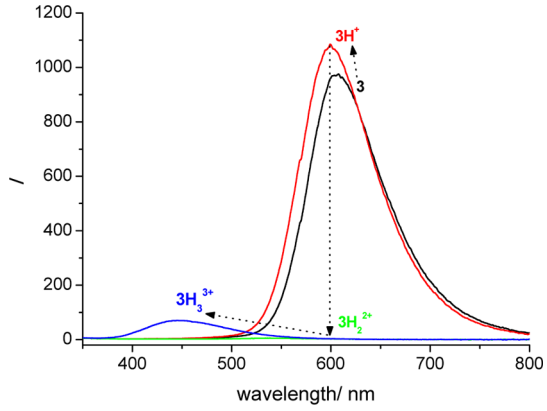

Figure 6. Fluorescence spectra of dye **3** (black line) with the addition of 1 equiv ($\mathbf{3H^+}$, red line), 2 equiv ($\mathbf{3H_2^{2+}}$, green line, nonfluorescent), and 20 equiv of TfOH ($\mathbf{3H_3^{3+}}$, blue line).

Implementation of Multilevel Logic Switches. The fluorescence modulation through proton-controlled PET and ICT processes makes the investigated dyes interesting candidates for the implementation of multivalued logic (see Table 2). Most logic switches work on the basis of binary principles, i.e., *high* (binary 1) and *low* (binary 0) signals. However, a strong interest in the design of switches that can differentiate between more than two levels for the input and output signals has recently evolved.[12] That is, for example, *low* (0), *medium* (1), and *high* (2) in the case of ternary switching. In this sense *off*−*on*−*off* switches differentiate three input signal levels: at a *low* input the switch is *off*, at *medium* input signal level an *on* state is observed, and at *high* input levels an *off* output again results. The design challenge lies in the precise control of orthogonal receptor sites which should trigger

dx.doi.org/10.1021/jo401147t | J. Org. Chem. 2013, 78, 7949−7961

Table 2. Truth Table for the Multivalued Switching of the BAI Dyes 1−4

	fluorescence output			
H^+ input[a]	dye **1** (λ_{obs} = 530 nm)[b]	dye **2** (λ_{obs} = 576 nm)[b]	dye **3** (λ_{obs} = 526 nm)[c,d]	dye **4** (λ_{obs} = 622 nm)[b,d]
0	0	1	2	1
1	1	2	3	1
2	0	0	0	0
3			1	
output:	binary	ternary	quaternary	binary
	off−on−off	*medium−on−off*		*on−off*

[a]The input levels 0, 1, and 2 indicate the number of equiv of TfOH; input level 3 (only applicable to dye **3**) corresponds to 20 equiv of TfOH. [b]Fluorescence maximum of the monoprotonated form of the dye. [c]Monitored at a wavelength where all forms (**3**, $3H^+$, $3H_2^{2+}$, and $3H_3^{3+}$) emit. [d]Monitoring the fluorescence output for **3** at 600 nm ($3H^+$) or for dye **4** at 580 nm (away from the maximum of any implied form) yields the reconfiguration of the switch toward an *on−off* (dye **3**) or *medium−on−off* (dye **4**) output signaling pattern.

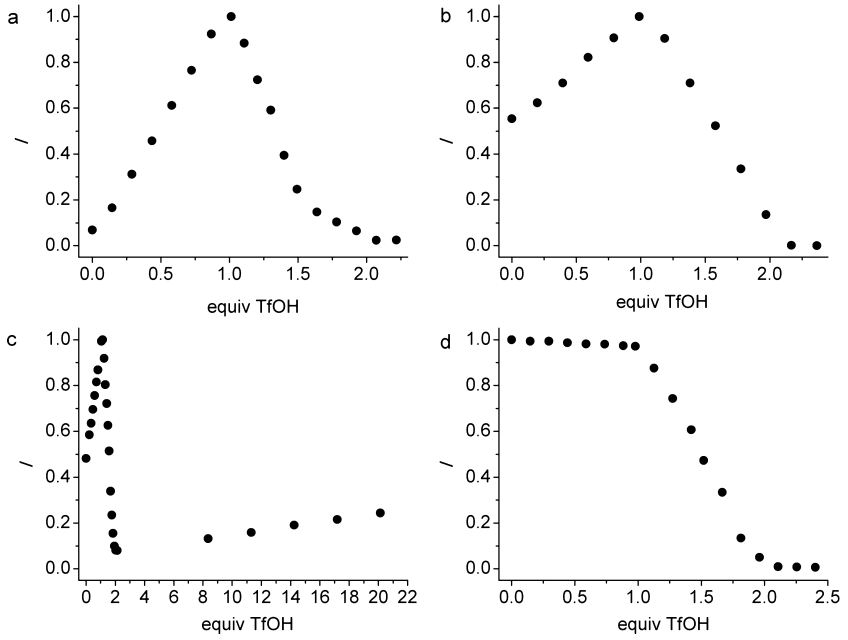

Figure 7. Fluorescence titration curves of dyes **1** (a), **2** (b), **3** (c), **4** (d) upon addition of TfOH. For observation wavelengths see Table 2.

opposing fluorescence modulation events (i.e., enhancement and quenching).

As results from the previously discussed protonation behavior of compound **1**, this dye fulfills these criteria, and thus it behaves as an *off−on−off* switch (see Table 2). The corresponding fluorescence titration monitored at the emission maximum of $1H^+$ is shown in Figure 7a. Furthermore, the proton inputs for each modulation (*off−on* and *on−off*) are degenerate (1 equiv of TfOH for each step), and therefore the switch is equally discussed as an XOR logic gate:[59] the presence of either (degenerate) proton input results in a high fluorescence, while the absence or simultaneous presence of both inputs yields a low fluorescence signal.

Dye **2**, in its nonprotonated state, showed a considerable fluorescence which was further increased upon the first protonation of the lateral N of the piperazinyl substituent. The second protonation, involving the isoquinolyl N, quenches the fluorescence quantitatively. Monitoring the fluorescence output at the maximum of the monoprotonated form $2H^+$ (see Figure 7b) led to the observation of a tristable switch with a *medium* (1)−*on* (2)−*off* (0) signal pattern. Here, both the input and output signals are represented by three discrete levels (see Table 2).

As discussed previously, dye **3** offers the possibility of three protonation steps, and therefore four states can be observed: **3**, $3H^+$, $3H_2^{2+}$, and $3H_3^{3+}$. These are differentiated by their emission quantum yields and in the case of the triprotonated form by a significantly different spectral position of the fluorescence. The choice of the emission maximum of the monoprotonated dye $3H^+$ at 600 nm as readout channel leads basically to a simple binary *on−off* switching. However, when selecting a strategic wavelength where all four forms of the dye have an emission response (526 nm), a four-level response (quaternary logic corresponding to 0, 1, 2, 3) was observed: **3** (level 2), $3H^+$ (level 3), $3H_2^{2+}$ (level 0), and $3H_3^{3+}$ (level 1) (see Figure 7c and Table 2). Such switches with fourfold stability are extremely rare.[39] Taking into account the pronounced spectral shift for the triprotonated dye **3**, the switching can be as well interpreted as *on−off−on′* modulation, where the two *on* situations correspond to different emission wavelengths (e.g., 600 and 447 nm). The realization of such functions has been described recently as nontrivial[60,61] and the herein described ICT dye **3** provides an interesting mechanistic extension for such switch types.

Finally, when monitoring the intensity at the emission maximum of the monoprotonated form of the anthracene-derived BAI dye **4**, a conventional *on−off* binary switch resulted

dx.doi.org/10.1021/jo401147t | J. Org. Chem. 2013, 78, 7949−7961

upon the addition of 2 equiv of protons (see Figure 7d and Table 2). Notably, by choosing the emission output channel at 580 nm (away from the emission maximum of any involved species), a *medium−on−off* pattern, as for dye **2**, was again observed. In summary, the investigated series of BAI dyes enables the possibility to adapt the switching behavior from binary via ternary to quaternary outputs by controlling the electronic properties through orthogonal protonation events. Notably, the initial level of fluorescence (and thereby the switching pattern for the first protonation step: *off-on* or *medium-on*) is a direct translation of the PET efficiency in the unprotonated dye. In turn the PET process can be reasonably controlled by fine-tuning electronic properties of the aryl residue, providing an interesting tool for the molecular design of multilevel switches.

CONCLUSIONS

The absorption and fluorescence properties of arylisoquinolines can be tuned by amino-substitution, the degree of π-conjugation of the aryl residue, and the presence of a boronic acid ester substituent. The prepared BAI dyes **1**−**4** constitute examples of efficient fluorophores that are based on ICT processes and that possess very characteristic emission fingerprints in the green to red spectral region. Furthermore, the presence of various basic groups enabled the observation of multiple and orthogonal protonation phenomena. This provided a convenient tool for achieving fluorescence enhancement as well as quenching by pH-induced switching. As a general observation, the protonation of the lateral amino N yielded hypsochromically shifted emission signatures along with increased quantum yields. The second protonation step of the less basic isoquinoline triggered a practically quantitative fluorescence quenching. In the case of dye **3**, a third protonation step was observed that manifested itself in a new emission band in the blue spectral region. The mechanistic explanation of the observed fluorescence modulation relies on the involvement of PET and the destabilization or stabilization of ICT states. For some of the protonated dyes, fluorescence quantum yields of up to 0.5 were obtained, increasing further the already quite appreciable quantum yields of the non-protonated dyes (ca. 0.2−0.4). The reading of the fluorescence response as output dependent on the proton input signals yielded a set of functional molecules with the potential of multilevel logic switching ranging from binary and ternary responses to extremely rare quaternary behavior. The implementation of such functions is of interest in the context of molecular logic-based computation.[12]

EXPERIMENTAL SECTION

Materials and Methods. ^{1}H NMR and ^{13}C NMR spectra were recorded at 400 or 500 MHz and 100 or 125 MHz, respectively, using the solvent peak for $CDCl_3$ as the internal reference (7.26 ppm and 77.0 ppm for ^{1}H and ^{13}C, respectively). ^{11}B NMR spectra were recorded with complete proton decoupling at 160 MHz using $BF_3{\cdot}Et_2O$ (0.00 ppm for ^{11}B NMR) as internal standard. Electrospray−ionization (EI) high-resolution mass spectra were recorded with a QTRAP mass spectrometer (hybrid triple quadrupole/linear ion trap mass spectrometer). Flash column chromatography was performed on silica gel (35−70 μm or 70−200 μm). Analytical thin-layer chromatography was done with aluminum backed plates (1.5 × 5.0 cm) precoated (0.25 mm) with silica gel. The compounds were visualized by exposure to UV light or by dipping the plates in a solution of 5% $(NH_4)_2Mo_7O_{24} \times 4H_2O$ in 95% ethanol (w/v), and then the plates were heated. Acetonitrile was of UV spectroscopic quality. Trifluoromethane sulfonic acid (triflic acid; TfOH; CF_3SO_3H, 98%) and phosphazene base P_2-Et (98%) were purchased from commercial suppliers and used as received.

All reactions were carried out by employing standard techniques in oven-dried Schlenk tubes under argon atmosphere. Anhydrous tetrahydrofuran (THF) was obtained using Grubbs-type solvent drying columns. Anhydrous 1,4-dioxane was obtained by distillation from sodium using benzophenone as indicator. Ethylacetate (EtOAc), methanol (MeOH), *n*-hexane, and dichloromethane (CH_2Cl_2) were purchased from commercial suppliers and used without further purification. Reagents, metallic precursors, and ligands for the syntheses were purchased from commercial suppliers and used as received. The only exceptions were 1-methylpiperazine and *N,N,N′*-trimethyl-1,3-propanediamine that were dried over CaH_2 and distilled before use. Potassium *tert*-butoxide was stored in a dry glovebox. The reagents 1-methyl-4-(naphthalen-1-yl)piperazine,[47] 1-chloroanthracene,[62] and 1-(8-methoxynaphthalen-1-yl)isoquinoline[43] were prepared following described methodologies.

Spectroscopic Measurements and Fluorescence Titrations. The dyes were tested for their nonprotonated state by adding 1 equiv phosphazene base P_2-Et, which in no case yielded significant changes in the UV−vis or fluorescence spectra. The TfOH stock solutions were calibrated by previous fluorescence titration (λ_{obs} = 416 nm) using recrystallized commercial 9-(*N*-methylamino)methylanthracene as indicator.[20]

All photophysical measurements were performed with air-equilibrated acetonitrile solutions at room temperature, using quartz cuvettes (1 cm optical path length). The UV−vis absorption spectra were obtained with a standard spectrophotometer. The fluorescence spectra were recorded with a fluorimeter equipped with a xenon flash lamp as excitation source and corrected for the spectral sensitivity of the photomultiplier detector. The fluorescence quantum yields were determined with quinine sulfate (Φ_f = 0.55 in 0.05 M sulfuric acid) as reference[63] and corrected for refractive index differences of the used solvents. The error margin of the quantum yields is estimated to be ±10% (except for dye **4** where it is ±20%).

The lifetime measurements were performed by means of time-correlated single photon counting with picosecond pulsed UV-LEDs (λ = 335 nm, pulse width fwhm 758 ps; λ = 338 nm, pulse width fwhm 625 ps; λ = 367 nm, pulse width fwhm 745 ps) or a picosecond pulsed diode laser (λ = 442 nm, pulse width fwhm 78 ps) as excitation sources. The error of the lifetimes is estimated to be ±5%.

The fluorescence titrations were performed by adding aliquots of a TfOH stock solution. The samples were excited at wavelengths where the changes in the UV−vis spectra were minimal in the course of the titration.

DFT Calculations. The calculations were made with the program Gaussian 03.[64] The ground-state geometries were optimized by applying the Kohn−Sham DFT. The B3LYP method with the 6-31+G(d,p) basis set was used for the full structural optimization and frequency calculations. The latter were done in order to verify the stationary points on the potential energy surface. For the calculations of the HOMO and LUMO frontier orbital energies, the TD-DFT at the B3LYP/6-31+G(d,p) level was applied.

Synthesis of Dyes and Their Precursors. 1-(4-Methoxyphenyl)isoquinoline A1. A Schlenk tube was charged with a solution of 1-chloroisoquinoline (327 mg, 2 mmol), 4-methoxyphenylboronic acid (365 mg, 2.4 mmol), Na_2CO_3 (424 mg, 4 mmol), and $Pd(PPh_3)_4$ (69 mg, 3 mol %). After three cycles of vacuum-argon flushing, toluene (2 mL), MeOH (0.4 mL), and H_2O (0.5 mL) were sequentially added. The reaction mixture was stirred at 110 °C overnight, then cooled to room temperature, quenched with H_2O (10 mL), and extracted with CH_2Cl_2 (3 × 20 mL). The organic layer was dried over anhydrous $MgSO_4$, filtered, concentrated, and the residue was purified by flash chromatography on silica gel (EtOAc/*n*-hexane 1:5) to give **A1** (430 mg, 91%) as a colorless solid. The spectroscopic data matched those reported in the literature.[65]

1-(4-(4-Methylpiperazin-1-yl)phenyl)isoquinoline M1. A solution of 1-methylpiperazine (144 μL, 1.3 mmol) in dry THF (1.0 mL) was stirred at 0 °C under argon. A solution of 2.5 M *n*-butyllithium in

dx.doi.org/10.1021/jo401147t | J. Org. Chem. 2013, 78, 7949−7961

n-hexane (0.52 mL, 1.3 mmol) was added dropwise through a septum. The reaction mixture was stirred at 0 °C for 30 min and then at room temperature for 1 h. Then **A1** (235 mg, 1.0 mmol) was added, and the reaction mixture was refluxed overnight. After it was cooled, the mixture was quenched with H_2O (10 mL) and extracted with CH_2Cl_2 (3 × 10 mL). The combined organic phase was dried over anhydrous Na_2SO_4, filtered, and concentrated to dryness. The crude product was purified by flash chromatography on silica gel (CH_2Cl_2/MeOH 20:1) to give **M1** (230 mg, 76%) as a pale yellow solid. mp 165−167 °C. ^{1}H NMR (400 MHz, $CDCl_3$): δ 8.58 (d, 1H, J = 5.7 Hz), 8.21 (d, 1H, J = 8.2 Hz), 7.87 (d, 1H, J = 8.2 Hz), 7.70−7.65 (m, 3H), 7.59 (d, 1H, J = 5.8 Hz), 7.53 (t, 1H, J = 8.0 Hz), 7.08 (d, 2H, J = 8.2 Hz), 3.35 (t, 4H, J = 4.8 Hz), 2.65 (t, 4H, J = 4.8 Hz), 2.40 (s, 3H). ^{13}C NMR (100 MHz, $CDCl_3$): δ 160.5, 151.4, 142.2, 137.0, 131.0, 130.6, 129.8, 127.8, 126.9, 126.9, 126.7, 119.2, 115.4, 55.0, 48.6, 46.1. HRMS (EI) m/z: M^+ calcd for $C_{20}H_{21}N_3$ 303.1735; found, 303.1744.

1-(4-Bromonaphthalen-1-yl)-4-methylpiperazine A2. Following the procedure described in the literature,[66] a solution of 1-methyl-4-(naphthalen-1-yl)piperazine (2.26 g, 10 mmol) in acetonitrile (60 mL) was treated with *N*-bromosuccinimide (1.96 g, 11 mmol), and the reaction mixture was stirred overnight at room temperature. Subsequently the reaction mixture was concentrated to dryness, and the resulting solid was extracted with an *n*-hexane/EtOAc 2:1 mixture (3 × 50 mL). After evaporation of the solvent, the crude product was purified by flash chromatography on silica gel (CH_2Cl_2/MeOH 20:1) to give **A2** (2.87 g, 94%) as a light brown solid: mp 92−94 °C. ^{1}H NMR (500 MHz, $CDCl_3$): δ 8.22 (d, 2H, J = 8.3 Hz), 7.68 (d, 1H, J = 8.0 Hz), 7.58 (t, 1H, J = 7.6 Hz), 7.53 (t, 1H, J = 7.6 Hz), 6.96 (d, 1H, J = 8.0 Hz), 3.13 (br s, 4H), 2.73 (br s, 4H), 2.43 (s, 3H). ^{13}C NMR (125 MHz, $CDCl_3$): δ 149.6, 132.8, 130.2, 129.7, 127.7, 127.2, 126.1, 124.0, 117.2, 115.5, 55.5, 52.9, 46.1. HRMS (EI) m/z: M^+ calcd for $C_{15}H_{17}BrN_2$ 304.0575 (^{79}Br), 306.0555 (^{81}Br); found, 304.0578 (^{79}Br), 306.0556 (^{81}Br).

1-(4-(4-Methylpiperazin-1-yl)naphthalen-1-yl)isoquinoline M2. Method A: Following a described procedure,[48] a dried Schlenk tube was charged with tris(dibenzylideneacetone)dipalladium(0) (Pd_2dba_3; 12 mg, 0.012 mmol), 2-dicyclohexylphosphino-2′,6′-dimethoxybiphenyl (SPhos; 39 mg, 0.096 mmol), bis(pinacolato)-diboron (B_2Pin_2; 305 mg, 1.2 mmol), **A2** (366 mg, 1.2 mmol), and KOAc (200 mg, 2.04 mmol). After three cycles of vacuum-argon flushing, 1,4-dioxane (4.0 mL) was added. The reaction mixture was heated to 110 °C for 6 h. At this point 1-chloroisoquinoline (163 mg, 1.0 mmol) in 1,4-dioxane (1.0 mL) and a 5 M aqueous solution of K_3PO_4 (1.0 mL) were added into the reaction flask. The mixture was heated to 110 °C overnight, cooled to room temperature, and diluted with H_2O (10 mL) and EtOAc (20 mL). The organic phase was separated, and the aqueous phase was extracted with EtOAc (3 × 20 mL). The combined organic phase was dried over anhydrous $MgSO_4$, filtered, and concentrated to dryness. Flash chromatography on silica gel (CH_2Cl_2/MeOH 15:1→5:1) gave **M2** (60 mg, 17%) as a light yellow foam. Method B: A solution of 1-methylpiperazine (72 μL, 0.65 mmol) in dry THF (0.5 mL) was stirred at 0 °C. A solution of 2.5 M *n*-butyllithium in *n*-hexane (0.260 mL, 0.65 mmol) was added dropwise. The reaction mixture was stirred at 0 °C for 30 min and then at room temperature for 1 h. Then 1-(8-methoxynaphthalen-1-yl)isoquinoline (143 mg, 0.5 mmol) was added, and the reaction mixture was refluxed overnight. After cooling, the mixture was quenched with H_2O (10 mL) and extracted with CH_2Cl_2 (3 × 10 mL). The combined organic phase was dried over anhydrous Na_2SO_4, filtered, and concentrated to dryness. The reaction crude was purified by flash chromatography on silica gel (CH_2Cl_2/MeOH 20:1) to give **M2** as light yellow foam (120 mg, 68%). ^{1}H NMR (400 MHz, $CDCl_3$): δ 8.72 (d, 1H, J = 5.7 Hz), 8.35 (d, 1H, J = 8.5 Hz), 7.95 (d, 1H, J = 8.3 Hz), 7.76 (d, 1H, J = 5.7 Hz), 7.72−7.68 (m, 2H), 7.55−7.48 (m, 2H), 7.45−7.42 (m, 2H), 7.33 (t, 1H, J = 8.3 Hz), 7.29 (d, 1H, J = 7.2 Hz), 3.29 (br s, 4H), 2.82 (br s, 4H), 2.50 (s, 3H). ^{13}C NMR (100 MHz, $CDCl_3$): δ 160.7, 150.2, 142.4, 136.5, 133.5, 132.3, 130.1, 128.9, 128.4, 127.9, 127.8, 127.0, 126.8, 126.5, 126.2, 125.3, 123.8, 120.0, 114.1, 55.6, 52.9, 46.2. HRMS (EI) m/z: M^+ calcd for $C_{24}H_{23}N_3$ 353.1892; found, 353.1894.

***N*-[4-(Isoquinolin-1-yl)naphthalen-1-yl]-*N*,*N*,*N*′-trimethylpropane-1,3-diamine M3.** A solution of *N*,*N*,*N*′-trimethyl-1,3-propanediamine (191 μL, 1.3 mmol) in dry THF (1 mL) was stirred at 0 °C under argon. A solution of 2.5 M *n*-butyllithium in *n*-hexane (0.52 mL, 1.3 mmol) was added dropwise through a septum. The reaction mixture was stirred at 0 °C for 30 min and then at room temperature for 1 h. Then 1-(8-methoxynaphthalen-1-yl)isoquinoline (285 mg, 1 mmol) was added, and the reaction mixture was refluxed overnight. After cooling, the mixture was quenched with H_2O (15 mL) and extracted with CH_2Cl_2 (3 × 10 mL). The combined organic phase was dried over Na_2SO_4, filtered, and concentrated to dryness. The reaction crude was purified by flash chromatography on silica gel (CH_2Cl_2/MeOH 10:1, 1% Et_3N) to give **M3** (270 mg, 73%) as a yellow-brown viscous oil. ^{1}H NMR (500 MHz, $CDCl_3$): δ 8.68 (d, 1H, J = 5.7 Hz), 8.35 (d, 1H, J = 8.4 Hz), 7.92 (d, 1H, J = 8.3 Hz), 7.73 (d, 1H, J = 5.7 Hz), 7.69−7.67 (m, 2H), 7.51−7.46 (m, 2H), 7.41 (t, 1H, J = 8.0 Hz), 7.39 (d, 1H, J = 8.0 Hz), 7.30 (t, 1H, J = 7.5 Hz), 7.25 (d, 1H, J = 8.3 Hz), 3.25 (t, 2H, J = 7.0 Hz), 2.94 (s, 3H), 2.59−2.48 (m, 2H), 2.35 (s, 6H), 1.97−1.91 (m, 2H). ^{13}C NMR (125 MHz, $CDCl_3$): δ 160.8, 150.6, 142.4, 136.5, 133.6, 132.2, 130.1, 129.8, 128.4, 127.9, 127.7, 127.1, 126.8, 126.5, 126.1, 125.3, 124.1, 120.0, 115.2, 57.4, 54.4, 45.0, 43.2, 25.0. HRMS (EI) m/z: M^+ calcd for $C_{25}H_{27}N_3$ 369.2205; found, 369.2208.

1-(Anthracen-1-yl)-4-methylpiperazine A4. A dried Schlenk tube was charged with palladium(II) acetate ($Pd(OAc)_2$; 3.8 mg, 0.017 mmol), SPhos (13.4 mg, 0.034 mmol), sodium *tert*-butoxide (226 mg, 2.35 mmol), and 1-chloroanthracene (357 mg, 1.68 mmol). After three consecutive cycles of vacuum-argon flushing, dry toluene (1.7 mL) and *N*-methylpiperazine (224 μL, 2.02 mmol) were added with the help of a syringe. The reaction mixture was heated to 60 °C for 2 h, cooled to room temperature, and diluted with H_2O (10 mL) and EtOAc (5 mL). The organic phase was separated, and the aqueous phase was extracted with EtOAc (3 × 10 mL). The combined organic phase was dried over anhydrous $MgSO_4$, filtered, and concentrated to dryness. The crude product was purified by flash chromatography on silica gel (CH_2Cl_2/MeOH 10:1) to give **A4** (400 mg, 86%) as a bright yellow viscous oil. ^{1}H NMR (500 MHz, $CDCl_3$): δ 8.76 (s, 1H), 8.41 (s, 1H), 8.05 (dd, 1H, J = 6.0, 2.0 Hz), 7.99 (dd, 1H, J = 6.0, 2.0 Hz), 7.71 (d, 1H, J = 8.5 Hz), 7.48−7.46 (m, 2H), 7.39 (t, 1H, J = 8.0 Hz), 7.05 (d, 1H, J = 7.5 Hz), 3.25 (br s, 4H), 2.81 (br s, 4H), 2.48 (s, 3H). ^{13}C NMR (125 MHz, $CDCl_3$): δ 149.5, 133.0, 131.5, 131.2, 128.7, 127.8, 127.6, 126.6, 125.4, 125.3, 125.1, 123.7, 122.4, 113.3, 55.7, 52.9, 46.2. HRMS (EI) m/z: M^+ calcd for $C_{19}H_{20}N_2$ 276.1626; found, 276.1627.

1-(4-Bromoanthracen-1-yl)-4-methylpiperazine B4. Following a described procedure,[66] a solution of **A4** (270 mg, 0.98 mmol) in acetonitrile (16 mL) was treated with *N*-bromosuccinimide (196 mg, 1.08 mmol), and the reaction mixture was stirred overnight at room temperature. Then the reaction mixture was concentrated to dryness, and the crude was purified by flash chromatography on silica gel (CH_2Cl_2/MeOH 20:1) to give **B4** (238 mg, 68%) as a yellow viscous oil. ^{1}H NMR (500 MHz, $CDCl_3$): δ 8.78 (s, 1H), 8.77 (s, 1H), 8.07 (m, 2H), 7.68 (d, 1H, J = 7.8 Hz), 7.53−7.51 (m, 2H), 6.87 (d, 1H, J = 7.8 Hz), 3.20 (br s, 4H), 2.80 (br s, 4H), 2.47 (s, 3H). ^{13}C NMR (125 MHz, $CDCl_3$): δ 149.7, 132.1, 131.4, 130.9, 129.1, 128.4, 128.3, 126.8, 126.1, 126.0, 123.2, 117.2, 113.8, 55.5, 53.0, 46.2. HRMS (EI) m/z: M^+ calcd for $C_{19}H_{19}BrN_2$ 354.0732 (^{79}Br), 356.0711 (^{81}Br); found, 354.0733 (^{79}Br), 356.0723 (^{81}Br).

1-(4-(4-Methylpiperazin-1-yl)anthracen-1-yl)isoquinoline M4. Following a described procedure,[48] a dried Schlenk tube was charged with Pd_2dba_3 (9.5 mg, 0.01 mmol), SPhos (31.5 mg, 0.08 mmol), B_2Pin_2 (251 mg, 0.99 mmol), **B4** (350 mg, 0.99 mmol), and KOAc (165 mg, 1.68 mmol). After three cycles of vacuum-argon flushing, 1,4-dioxane (3.4 mL) was added with the help of a syringe. Then the reaction mixture was heated overnight to 110 °C. Subsequently 1-chloroisoquinoline (134 mg, 0.83 mmol) dissolved in 1,4-dioxane (1.0 mL) and 5 M aqueous solution of K_3PO_4 (0.8 mL) were added by a syringe into the reaction flask. The reaction mixture was heated to 110 °C for 10 h, cooled to room temperature, and diluted with H_2O (10 mL) and EtOAc (20 mL). The organic phase was separated and the aqueous phase was extracted with EtOAc (3 ×

dx.doi.org/10.1021/jo401147t | J. Org. Chem. 2013, 78, 7949−7961

20 mL). The combined organic phase was dried over anhydrous $MgSO_4$, filtered, and concentrated to dryness. Flash chromatography on silica gel (CH_2Cl_2/MeOH 20:1→10:1) gave **M4** (105 mg, 31%) as a yellow-orange foam. ^{1}H NMR (500 MHz, $CDCl_3$): δ 8.86 (s, 1H), 8.74 (d, 1H, J = 5.5 Hz), 8.04 (d, 1H, J = 8.0 Hz), 7.96 (s, 1H), 7.95 (d, 1H, J = 7.0 Hz), 7.79 (d, 1H, J = 5.5 Hz), 7.73−7.66 (m, 3H), 7.48 (d, 1H, J = 7.5 Hz), 7.43 (t, 1H, J = 8.0 Hz), 7.39 (t, 1H, J = 8.0 Hz), 7.34 (t, 1H, J = 7.5 Hz), 7.18 (d, 1H, J = 7.5 Hz), 3.36 (br s, 4H), 2.89 (br s, 4H), 2.53 (s, 3H). ^{13}C NMR (125 MHz, $CDCl_3$): δ 160.8, 150.2, 142.5, 136.6, 132.4, 132.0, 131.6, 131.1, 130.2, 128.6, 128.5, 128.3, 127.9, 127.6, 127.5, 127.1, 126.9, 125.5, 125.4, 122.7, 120.1, 112.8, 55.7, 52.9, 46.2. HRMS (EI) m/z: M^+ calcd for $C_{28}H_{25}N_3$ 403.2048; found, 403.2058.

General Procedure for the Ir-Catalyzed Borylation. Following a recently described method,[49] a dried Schlenk tube was charged with the substrate (**M1**, **M2**, **M3** or **M4**) and B_2Pin_2 (1 equiv). After three cycles of vacuum-argon flushing, 1 mL of catalyst stock solution[67] per 0.5 mmol of substrate and pinacolborane (HBPin; 5 mol %) were added. The reaction mixture was stirred at 55−80 °C until reaching quantitative consumption of the starting material (as indicated by TLC monitoring). The mixture was cooled to room temperature, concentrated to dryness, and the crude products were purified by column chromatography (CH_2Cl_2/MeOH mixtures).

1-[4-(4-Methylpiperazin-1-yl)-2-(4,4,5,5-tetramethyl-1,3,2-dioxaborolan-2-yl)phenyl]isoquinoline 1. Following the previously described general procedure for Ir-catalyzed borylation, starting from **M1** (76 mg, 0.25 mmol) and carrying out the reaction at 80 °C, flash chromatography on silica gel (CH_2Cl_2/MeOH 10:1) gave **1** (95 mg, 89%) as an orange foam. ^{1}H NMR (400 MHz, $CDCl_3$): δ 8.82 (d, 1H, J = 8.2 Hz), 8.42 (d, 1H, J = 6.3 Hz), 8.12 (d, 1H, J = 8.6 Hz), 7.85 (d, 1H, J = 8.2 Hz), 7.77 (t, 1H, J = 8.0 Hz), 7.67 (t, 1H, J = 8.0 Hz), 7.51 (d, 1H, J = 6.3 Hz), 7.32 (d, 1H, J = 2.7 Hz), 6.83 (dd, 1H, J = 8.6, 2.7 Hz), 3.43−3.40 (m, 4H), 2.60−2.57 (m, 4H), 2.36 (s, 3H), 1.41 (s, 12H, 4 × CH_3). ^{13}C NMR (100 MHz, $CDCl_3$): δ 157.6, 153.0, 139.0, 134.5, 132.1, 129.7, 128.3, 127.5, 127.4, 125.1, 119.0, 117.3, 114.0, 80.1, 55.0, 47.8, 46.1, 27.3, (*C*−B not observed).^{11}B NMR (160 MHz, $CDCl_3$): δ 13.0 (br s) ppm; HRMS (EI) m/z: M^+ calcd for $C_{26}H_{32}BN_3O_2$ 429.2588; found, 429.2575.

1-[4-(4-Methylpiperazin-1-yl)-2-(4,4,5,5-tetramethyl-1,3,2-dioxaborolan-2-yl)naphthalen-1-yl]isoquinoline 2. Following the previously described general procedure for Ir-catalyzed borylation, starting from **M2** (71 mg, 0.2 mmol) and carrying out the reaction at 55 °C, flash chromatography on silica gel (CH_2Cl_2/MeOH 10:1) gave **2** (58 mg, 61%) as a yellow foam. ^{1}H NMR (400 MHz, $CDCl_3$): δ 8.64 (d, 1H, J = 5.6 Hz), 8.29 (d, 1H, J = 8.8 Hz), 7.87 (d, 1H, J = 8.0 Hz), 7.70 (d, 1H, J = 5.6 Hz), 7.61 (td, 1H, J = 7.4, 1.2 Hz), 7.54 (s, 1H), 7.49 (d, 1H, J = 8.4 Hz), 7.48 (td, 1H, J = 7.6, 1.6 Hz), 7.34−7.24 (m, 3H), 3.28 (br s, 4H), 2.78 (br s, 4H), 2.46 (s, 3H), 0.92 (s, 6H), 0.74 (s, 6H). ^{13}C NMR (100 MHz, $CDCl_3$): δ 162.1, 148.9, 142.0, 139.7, 136.0, 133.6, 130.2, 129.9, 129.6, 127.7, 127.4, 126.6, 126.4, 126.1, 125.9, 123.5, 119.3, 118.9, 83.1, 55.7, 52.8, 46.3, 24.4, 24.1, (*C*−B not observed). ^{11}B NMR (160 MHz, $CDCl_3$): δ 31.1 (br s) ppm; HRMS (EI) m/z: M^+ calcd for $C_{30}H_{34}BN_3O_2$ 479.2744; found, 479.2754.

***N*-[4-(Isoquinolin-1-yl)-3-(4,4,5,5-tetramethyl-1,3,2-dioxaborolan-2-yl)naphthalen-1-yl]-*N*,*N*,*N*′-trimethylpropane-1,3-diamine 3.** Following the previously described general procedure for Ir-catalyzed borylation, starting from **M3** (92 mg, 0.25 mmol) and carrying out the reaction at 80 °C, flash chromatography on silica gel (CH_2Cl_2/MeOH 10:1, 1% Et_3N) gave **3** (71 mg, 58%) as an orange viscous oil. Note: The product may be contaminated with Et_3NHCl that can be removed washing a CH_2Cl_2 solution of the product with a saturated aqueous $NaHCO_3$ solution. ^{1}H NMR (400 MHz, $CDCl_3$): δ 8.64 (d, 1H, J = 5.7 Hz), 8.34 (d, 1H, J = 8.5 Hz), 7.87 (d, 1H, J = 8.2 Hz), 7.70 (d, 1H, J = 5.7 Hz), 7.61 (t, 1H, J = 7.6 Hz), 7.56 (s, 1H), 7.48−7.45 (m, 2H), 7.32 (t, 1H, J = 7.6 Hz), 7.29−7.24 (m, 2H), 3.22 (t, 2H, J = 7.3 Hz), 2.96 (s, 3H), 2.41−2.37 (m, 2H), 2.25 (s, 6H), 1.92−1.87 (m, 2H), 0.92 (s, 6H), 0.74 (s, 6H). ^{13}C NMR (100 MHz, $CDCl_3$): δ 162.2, 149.8, 141.9, 139.4, 136.0, 133.6, 131.1, 129.9, 129.6, 127.8, 127.3, 126.6, 126.3, 126.0, 125.8, 123.9, 120.0, 119.3, 83.1, 57.7, 55.0, 45.5, 42.8, 25.9, 24.4, 24.1, (*C*−B not observed). ^{11}B NMR (160 MHz, $CDCl_3$): δ 32.2 (br s) ppm; HRMS (EI) m/z: M^+ calcd for $C_{31}H_{38}BN_3O_2$ 495.3057; found, 495.3054.

1-[4-(4-Methylpiperazin-1-yl)-2-(4,4,5,5-tetramethyl-1,3,2-dioxaborolan-2-yl)anthracen-1-yl]isoquinoline 4. Following the previously described general procedure for Ir-catalyzed borylation, starting from **M4** (84 mg, 0.21 mmol) and carrying out the reaction at 55 °C, flash chromatography on silica gel (CH_2Cl_2/MeOH 10:1) gave **4** (89 mg, 80%) as an orange foam. ^{1}H NMR (500 MHz, $CDCl_3$): δ 8.82 (s, 1H), 8.69 (d, 1H, J = 5.7 Hz), 8.02 (d, 1H, J = 8.6 Hz), 7.91 (d, 1H, J = 8.2 Hz), 7.87 (s, 1H), 7.76 (d, 1H, J = 5.7 Hz), 7.66−7.61 (m, 2H), 7.51 (d, 1H, J = 8.5 Hz), 7.47 (s, 1H), 7.42 (t, 1H, J = 7.5 Hz), 7.33−7.29 (m, 2H), 3.39 (br s, 4H), 2.89 (br s, 4H), 2.53 (s, 3H), 0.94 (s, 6H), 0.75 (s, 6H). ^{13}C NMR (125 MHz, $CDCl_3$): δ 162.1, 148.6, 142.1, 140.5, 136.1, 132.2, 131.6, 131.4, 130.0, 129.6, 128.6, 128.5, 128.3, 127.7, 126.8, 126.6, 126.4, 125.7, 125.2, 122.2, 119.5, 117.1, 83.2, 55.7, 52.7, 46.2, 24.4, 24.1, (*C*−B not observed). ^{11}B NMR (160 MHz, $CDCl_3$): δ 32.2 (br s) ppm; HRMS (EI) m/z: M^+ calcd for $C_{34}H_{36}N_3O_2B$ 529.2901; found, 529.2915.

■ ASSOCIATED CONTENT

Ⓢ Supporting Information

^{1}H NMR spectrum of **A1**, ^{1}H and ^{13}C NMR spectra of **A2**, **A4**, **B4**, **M1**−**M4**, and **1**−**4**, UV−vis absorption and fluorescence spectra of the compounds **M1**−**M4**, ^{11}B NMR spectra of dye **1** upon protonation, UV−vis absorption and fluorescence spectra of dyes **2**−**4** upon titration with TfOH, photophysical properties of the compounds **M1**−**M4**, optimized ground-state geometries and calculation details for dyes **1**−**4**, LUMO+1 contour plot of dye **4**, and solvatochromic shifts of the emission of dye **4**. This material is available free of charge via the Internet at http://pubs.acs.org.

■ AUTHOR INFORMATION

Corresponding Author

*E-mail: abel.ros@iiq.csic.es, uwe.pischel@diq.uhu.es.

Notes

The authors declare no competing financial interest.

■ ACKNOWLEDGMENTS

This work was funded by the Spanish Ministry for Economy and Competitiveness (Grants CTQ2011-28390 for U.P., CTQ2010-15297 and CTQ2010-14974 for A.R., Ph.D. fellowship for R.L-R.), European FEDER funds, and the Junta de Andalucía (Grants 2008/FQM-3685 for U.P., 2008/FQM-3833 and 2009/FQM-4537 for A.R., Ph.D. fellowship for V.F.P.). A.R. acknowledges the European Union for a Marie Curie Reintegration Grant (FP7-PEOPLE-2009-RG-256461) and the Consejo Superior de Investigaciones Científicas (CSIC, Madrid) for a JAE-Doc Fellowship. H.S.E.-S. thanks the Computational Laboratory for Analysis, Modeling, and Visualization at the Jacobs University Bremen (Germany) for computation time.

■ REFERENCES

(1) de Silva, A. P.; Gunaratne, H. Q. N.; Gunnlaugsson, T.; Huxley, A. J. M.; McCoy, C. P.; Rademacher, J. T.; Rice, T. E. *Chem. Rev.* **1997**, *97*, 1515−1566.

(2) Martínez-Máñez, R.; Sancenón, F. *Chem. Rev.* **2003**, *103*, 4419−4476.

(3) Anslyn, E. V. *J. Org. Chem.* **2007**, *72*, 687−699.

(4) de Silva, A. P.; Vance, T. P.; West, M. E. S.; Wright, G. D. *Org. Biomol. Chem.* **2008**, *6*, 2468−2480.

(5) Guo, Z.; Shin, I.; Yoon, J. *Chem. Commun.* **2012**, *48*, 5956−5967.

(6) de Silva, A. P.; Uchiyama, S. *Nat. Nanotechnol.* **2007**, *2*, 399−410.

(7) Pischel, U. *Angew. Chem., Int. Ed.* **2007**, *46*, 4026−4040.
(8) Credi, A. *Angew. Chem., Int. Ed.* **2007**, *46*, 5472−5475.
(9) Szaciłowski, K. *Chem. Rev.* **2008**, *108*, 3481−3548.
(10) Tian, H. *Angew. Chem., Int. Ed.* **2010**, *49*, 4710−4712.
(11) Andréasson, J.; Pischel, U. *Chem. Soc. Rev.* **2010**, *39*, 174−188.
(12) de Silva, A. P. *Molecular Logic-Based Computation*; The Royal Society of Chemistry: Cambridge, U.K., 2012.
(13) de Ruiter, G.; Motiei, L.; Choudhury, J.; Oded, N.; van der Boom, M. E. *Angew. Chem., Int. Ed.* **2010**, *49*, 4780−4783.
(14) de Silva, A. P.; Gunaratne, H. Q. N.; McCoy, C. P. *Chem. Commun.* **1996**, *21*, 2399−2400.
(15) de Silva, S. A.; Zavaleta, A.; Baron, D. E.; Allam, O.; Isidor, E. V.; Kashimura, N.; Percarpio, J. M. *Tetrahedron Lett.* **1997**, *38*, 2237−2240.
(16) Albelda, M. T.; Bernardo, M. A.; García-España, E.; Godino-Salido, M. L.; Luis, S. V.; Melo, M. J.; Pina, F.; Soriano, C. *J. Chem. Soc., Perkin Trans. 2* **1999**, 2545−2549.
(17) de Silva, S. A.; Amorelli, B.; Isidor, D. C.; Loo, K. C.; Crooker, K. E.; Pena, Y. E. *Chem. Commun.* **2002**, 1360−1361.
(18) Callan, J. F.; de Silva, A. P.; Ferguson, J.; Huxley, A. J. M.; O'Brien, A. M. *Tetrahedron* **2004**, *60*, 11125−11131.
(19) Chen, Y. T.; Wang, H. L.; Wan, L.; Bian, Y. Z.; Jiang, J. Z. *J. Org. Chem.* **2011**, *76*, 3774−3781.
(20) Pais, V. F.; Remón, P.; Collado, D.; Andréasson, J.; Pérez-Inestrosa, E.; Pischel, U. *Org. Lett.* **2011**, *13*, 5572−5575.
(21) Shiraishi, Y.; Miyamoto, R.; Hirai, T. *Tetrahedron Lett.* **2007**, *48*, 6660−6664.
(22) Brown, G. J.; de Silva, A. P.; James, M. R.; McKinney, B. O. F.; Pears, D. A.; Weir, S. M. *Tetrahedron* **2008**, *64*, 8301−8306.
(23) Jiang, J. B.; Leng, B.; Xiao, X.; Zhao, P.; Tian, H. *Polymer* **2009**, *50*, 5681−5684.
(24) Diaz-Fernandez, Y.; Foti, F.; Mangano, C.; Pallavicini, P.; Patroni, S.; Perez-Gramatges, A.; Rodriguez-Calvo, S. *Chem.—Eur. J.* **2006**, *12*, 921−930.
(25) Pallavicini, P.; Diaz-Fernandez, Y. A.; Pasotti, L. *Analyst* **2009**, *134*, 2147−2152.
(26) Denat, F.; Diaz-Fernandez, Y. A.; Pasotti, L.; Sok, N.; Pallavicini, P. *Chem.—Eur. J.* **2010**, *16*, 1289−1295.
(27) Fabbrizzi, L.; Licchelli, M.; Parodi, L.; Poggi, A.; Taglietti, A. *Eur. J. Inorg. Chem.* **1999**, 35−39.
(28) Amendola, V.; Fabbrizzi, L.; Mangano, C.; Miller, H.; Pallavicini, P.; Perotti, A.; Taglietti, A. *Angew. Chem., Int. Ed.* **2002**, *41*, 2553−2556.
(29) Gunnlaugsson, T.; Leonard, J. P.; Sénéchal, K.; Harte, A. J. *J. Am. Chem. Soc.* **2003**, *125*, 12062−12063.
(30) Aucejo, R.; Alarcón, J.; García-España, E.; Llinares, J. M.; Marchin, K. L.; Soriano, C.; Lodeiro, C.; Bernardo, M. A.; Pina, F.; Pina, J.; Seixas de Melo, J. *Eur. J. Inorg. Chem.* **2005**, 4301−4308.
(31) Han, M.-J.; Gao, L.-H.; Lü, Y.-Y.; Wang, K.-Z. *J. Phys. Chem. B* **2006**, *110*, 2364−2371.
(32) Yao, J.-L.; Gao, X.; Sun, W. L.; Fan, X.-Z.; Shi, S.; Yao, T.-M. *Inorg. Chem.* **2012**, *51*, 12591−12593.
(33) Pina, F.; Melo, M. J.; Maestri, M.; Passaniti, P.; Balzani, V. *J. Am. Chem. Soc.* **2000**, *122*, 4496−4498.
(34) Andréasson, J.; Straight, S. D.; Kodis, G.; Park, C. D.; Hambourger, M.; Gervaldo, M.; Albinsson, B.; Moore, T. A.; Moore, A. L.; Gust, D. *J. Am. Chem. Soc.* **2006**, *128*, 16259−16265.
(35) Evangelio, E.; Hernando, J.; Imaz, I.; Bardají, G. G.; Alibés, R.; Busqué, F.; Ruiz-Molina, D. *Chem.—Eur. J.* **2008**, *14*, 9754−9763.
(36) Sadhu, K. K.; Mizukami, S.; Yoshimura, A.; Kikuchi, K. *Org. Biomol. Chem.* **2013**, *11*, 563−568.
(37) Lee, H. Y.; Olasz, A.; Chen, C.-H.; Lee, D. *Org. Lett.* **2012**, *14*, 6286−6289.
(38) Ferreira, R.; Remón, P.; Pischel, U. *J. Phys. Chem. C* **2009**, *113*, 5805−5811.
(39) Di Pietro, C.; Guglielmo, G.; Campagna, S.; Diotti, M.; Manfredi, A.; Quici, S. *New J. Chem.* **1998**, *22*, 1037−1039.
(40) Fabbrizzi, L.; Licchelli, M.; Pallavicini, P.; Parodi, L. *Angew. Chem., Int. Ed.* **1998**, *37*, 800−802.
(41) Pina, F.; Melo, M. J.; Bernardo, M. A.; Luis, S. V.; García-España, E. *J. Photochem. Photobiol. A* **1999**, *126*, 65−69.
(42) Dilek, G.; Akkaya, E. U. *Tetrahedron Lett.* **2000**, *41*, 3721−3724.
(43) Pais, V. F.; El-Sheshtawy, H. S.; Fernández, R.; Lassaletta, J. M.; Ros, A.; Pischel, U. *Chem.—Eur. J.* **2013**, *19*, 6650−6661.
(44) Hudson, Z. M.; Wang, S. *Acc. Chem. Res.* **2009**, *42*, 1584−1596.
(45) Wade, C. R.; Broomsgrove, A. E. J.; Aldridge, S.; Gabbaï, F. P. *Chem. Rev.* **2010**, *110*, 3958−3984.
(46) Hudson, Z. M.; Liu, X.-Y.; Wang, S. *Org. Lett.* **2011**, *13*, 300−303.
(47) ten Hoeve, W.; Kruse, C. G.; Luteyn, J. M.; Thiecke, J. R. G.; Wynberg, H. *J. Org. Chem.* **1993**, *58*, 5101−5106.
(48) Billingsley, K. L.; Barder, T. E.; Buchwald, S. L. *Angew. Chem., Int. Ed.* **2007**, *46*, 5359−5363.
(49) Ros, A.; Estepa, B.; López-Rodríguez, R.; Álvarez, E.; Fernández, R.; Lassaletta, J. M. *Angew. Chem., Int. Ed.* **2011**, *50*, 11724−11728.
(50) López-Rodríguez, R.; Ros, A.; Fernández, R.; Lassaletta, J. M. *J. Org. Chem.* **2012**, *77*, 9915−9920.
(51) Ros, A.; López-Rodríguez, R.; Estepa, B.; Álvarez, E.; Fernández, R.; Lassaletta, J. M. *J. Am. Chem. Soc.* **2012**, *134*, 4573−4576.
(52) Zhu, L.; Shabbir, S. H.; Gray, M.; Lynch, V. M.; Sorey, S.; Anslyn, E. V. *J. Am. Chem. Soc.* **2006**, *128*, 1222−1232.
(53) Khalili, F.; Henni, A.; East, A. L. L. *J. Chem. Eng. Data* **2009**, *54*, 2914−2917.
(54) Zieliński, W.; Kudelko, A. *Arkivoc* **2005**, *(V)*, 66−82.
(55) Mantina, M.; Chamberlin, A. C.; Valero, R.; Cramer, C. J.; Truhlar, D. G. *J. Phys. Chem. A* **2009**, *113*, 5806−5812.
(56) In accordance with the postulated ICT character of the fluorescence of dye **4** a red shift of the emission maximum in solvents of increasing polarity was observed: $\lambda_{f,\,max}$ = 601 nm in *n*-hexane, 629 nm in THF, 638 nm in acetonitrile and *N*,*N*-dimethylformamide.
(57) de Silva, A. P.; Gunaratne, H. Q. N.; Habib-Jiwan, J.-L.; McCoy, C. P.; Rice, T. E.; Soumillion, J.-P. *Angew. Chem., Int. Ed. Engl.* **1995**, *34*, 1728−1731.
(58) Rehm, D.; Weller, A. *Ber. Bunsen. Phys. Chem.* **1969**, *73*, 834−839.
(59) Credi, A.; Balzani, V.; Langford, S. J.; Stoddart, J. F. *J. Am. Chem. Soc.* **1997**, *119*, 2679−2681.
(60) Luxami, V.; Kumar, S. *Tetrahedron Lett.* **2007**, *48*, 3083−3087.
(61) Amendola, V.; Bergamaschi, G.; Boiocchi, M.; Fabbrizzi, L.; Mosca, L. *J. Am. Chem. Soc.* **2013**, *135*, 6345−6355.
(62) Moursounidis, J.; Wege, D. *Aust. J. Chem.* **1988**, *41*, 235−249.
(63) Morris, J. V.; Mahaney, M. A.; Huber, J. R. *J. Phys. Chem.* **1976**, *80*, 969−974.
(64) Frisch, M. J.; Trucks, G. W.; Schlegel, H. B.; Scuseria, G. E.; Robb, M. A.; Cheeseman, J. R.; Montgomery, Jr., J. A.; Vreven, T.; Kudin, K. N.; Burant, J. C.; Millam, J. M.; Iyengar, S. S.; Tomasi, J.; Barone, V.; Mennucci, B.; Cossi, M.; Scalmani, G.; Rega, N.; Petersson, G. A.; Nakatsuji, H.; Hada, M.; Ehara, M.; Toyota, K.; Fukuda, R.; Hasegawa, J.; Ishida, M.; Nakajima, T.; Honda, Y.; Kitao, O.; Nakai, H.; Klene, M.; Li, X.; Knox, J. E.; Hratchian, H. P.; Cross, J. B.; Bakken, V.; Adamo, C.; Jaramillo, J.; Gomperts, R.; Stratmann, R. E.; Yazyev, O.; Austin, A. J.; Cammi, R.; Pomelli, C.; Ochterski, J. W.; Ayala, P. Y.; Morokuma, K.; Voth, G. A.; Salvador, P.; Dannenberg, J. J.; Zakrzewski, V. G.; Dapprich, S.; Daniels, A. D.; Strain, M. C.; Farkas, O.; Malick, D. K.; Rabuck, A. D.; Raghavachari, K.; Foresman, J. B.; Ortiz, J. V.; Cui, Q.; Baboul, A. G.; Clifford, S.; Cioslowski, J.; Stefanov, B. B.; Liu, G.; Liashenko, A.; Piskorz, P.; Komaromi, I.; Martin, R. L.; Fox, D. J.; Keith, T.; Al-Laham, M. A.; Peng, C. Y.; Nanayakkara, A.; Challacombe, M.; Gill, P. M. W.; Johnson, B.; Chen, W.; Wong, M. W.; Gonzalez, C.; and Pople, J. A.; *Gaussian 03, Revision E.01*, Gaussian, Inc.: Wallingford CT, 2004.
(65) Dong, J.; Shi, X.-X.; Yan, J.-J.; Xing, J.; Zhang, Q.; Xiao, S. *Eur. J. Org. Chem.* **2010**, 6987−6992.
(66) Carreño, M. C.; García-Ruano, J. L.; Sanz, G.; Toledo, M. A.; Urbano, A. *J. Org. Chem.* **1995**, *60*, 5328−5331.
(67) The catalyst stock solution (25 mL) was prepared by dissolving 2-pyridinecarboxaldehyde *N*,*N*-dibenzylhydrazone (37.6 mg, 0.125 mmol) and $[Ir(\mu\text{-OMe})(cod)]_2$ (41 mg, 0.063 mmol) in dry

tetrahydrofuran. Sonication for 1 h was used to facilitate dissolution. The resulting red-brown solution was kept under argon.

dx.doi.org/10.1021/jo401147t | J. Org. Chem. 2013, 78, 7949−7961